# In-Vivo Comparison of Multiline Transmission and Diverging Wave Imaging for High Frame Rate Speckle Tracking Echocardiography

# In-Vivo Comparison of Multiline Transmission and Diverging Wave Imaging for High Frame Rate Speckle Tracking Echocardiography

Marta Orlowska, Alessandro Ramalli, Stéphanie Bézy, Valentino Meacci, Jens-Uwe Voigt and Jan D'hooge

***Abstract*— High frame rate (HFR) speckle tracking echocardiography (STE) assesses myocardial function by quantifying motion and deformation at high temporal resolution. Among the proposed HFR techniques, Multi-Line Transmission (MLT) and Diverging Wave (DW) imaging have been used in this context both being characterized by specific advantages and disadvantages. Therefore, in this paper, we directly contrast both approaches in an in-vivo setting while operating at the same frame rate. First, images were recorded at baseline (resting condition) from healthy volunteers and patients. Next, additional acquisitions during stress echocardiography were performed on volunteers. Each scan was contoured and processed by a previously proposed 2D HFR STE algorithm based on cross-correlation. Then, strain curves and their end-systolic (ES) values were extracted for all myocardial segments for further statistical analysis. The baseline acquisitions did not reveal differences in estimated strain between the acquisition modes ($p>0.35$); myocardial segments ($p>0.3$) nor an interaction between imaging mode and depth ($p>0.87$). Similarly, during stress testing, no difference ($p=0.7$) was observed for the two scan sequences, stress levels nor an interaction sequence-stress level ($p=0.94$). Overall, our findings show that MLT and DW compounding give comparable HFR STE strain values and that the choice for using one method or the other may thus rather be based on other factors, e.g. system requirements or computational cost.**

***Index Terms*—Speckle tracking, high frame rate, multiline transmission, diverging waves, echocardiography, in-vivo images.**

## I. Introduction

The non-invasive quantification of myocardial function is an important goal in clinical cardiology [1], [2]. Among the techniques to assess myocardial function [3]–[7], speckle tracking echocardiography (STE), which allows a semi-automatic and angle-independent quantification of myocardial deformation, has been shown useful in a multitude of cardiac conditions [8]–[11]. However, in current clinical practice, STE is based on conventional B-mode imaging at relatively low frame rate (FR), i.e. typically lower than 80Hz, thereby limiting the time resolution of cardiac mechanics' assessment. With the available FR some of the cardiac mechanical phases, which are known to be associated with very fast motion and deformation of the myocardium, cannot be studied accurately, although they might contain potentially important information on cardiac (patho-)physiology. As an example, in a healthy heart, the left ventricular depolarization and the associated mechanical activation typically last only 30ms. Disturbances of the normal activation pattern can result in dyssynchronous – and therefore less efficient – cardiac contraction, which can be corrected for by pacemaker therapy [12]–[14]. Hence, it would be of both diagnostic and therapeutic benefit to be able to study short-lived cardiac phases in detail.

Lately, multiple authors have presented new approaches towards high frame rate (HFR) ultrasound imaging of the heart [15] to allow better assessment of cardiac function. For instance, Kanai et al. applied a relatively straightforward approach by sacrificing spatial resolution and field of view in favor of temporal resolution by reducing the number of lines in the 2D image [16]. On the other hand, massive parallel receive beam forming [17], also called Multiline Acquisition (MLA), reconstructs multiple image lines from a single defocused transmission to keep the field of view wide and to increase the time resolution at the same time. Hereto, it is required to transmit a very broad ultrasound beam - plane wave (PW) or diverging wave (DW) - instead of the traditionally used focused beams [18]–[26]. However, due to the width of the transmitted beam, this approach results in images with limited spatial resolution, contrast, and signal-to-noise ratio (SNR). Spatial coherent compounding of multiple images, obtained from broad beams steered along different directions, has been proposed to improve image quality, but at the expense of the final frame rate and with limitations due to cardiac motion [18]. The high temporal resolution achievable with DWs have been already exploited to develop and in-vivo test novel specific STE algorithms [23], [27]–[29]. Nevertheless, Tong et al. proposed an alternative cardiac imaging technique, based on the

M. Orlowska was supported by FWO grants No G002617N and G092318N. JU. Voigt holds an personal FWO research mandate 1832917N. A. Ramalli was supported by the European Union's Horizon 2020 research and innovation programme under the Marie Skłodowska-Curie grant agreement No 786027 (ACOUSTIC project). S. Bézy was supported by FWO grant No G092318N.

M. Orlowska and J. D'hooge are with the Laboratory of Cardiovascular Imaging and Dynamics, Department of Cardiovascular Sciences, KU Leuven, 3000 Leuven, Belgium.

A. Ramalli is with the Department of Information Engineering, University of Florence, 50139, Florence, Italy, but he was with the Laboratory of Cardiovascular Imaging and Dynamics, Department of Cardiovascular Sciences, KU Leuven, 3000 Leuven, Belgium when the work was done.

S. Bézy, and J.U. Voigt are with Department of Cardiovascular Sciences, University of Leuven, Leuven, Belgium and Department of Cardiovascular Diseases, University Hospitals Leuven, Leuven, Belgium.

V. Meacci is with the Department of Information Engineering, University of Florence, 50139, Florence, Italy.

simultaneous transmission of multiple focused beams along different steering direction [30], referred to as multiline transmission (MLT), which, in combination with MLA, allows achieving frame rates comparable to those achieved with DWs [31]–[35]. Nevertheless, even if MLT improves the spatial resolution w.r.t. DW compounding, images still suffer from low SNR and contrast due to potential cross talk between the MLT beams despite the multiple mitigation schemes that were proposed [35]–[37].

Since DW and MLT approaches have different advantages and disadvantages in terms of system requirements, computational load, energy transfer to the body, achievable frame rate, motion artifacts and not least, image quality, they were compared in different applications, e.g. in HFR color Doppler [38] and HFR tri-plane echocardiography [39]. Specifically for HFR STE, MLT and DW imaging were compared in [40] in terms of image quality, motion artifacts, and their effects on motion estimation when using a STE algorithm based on normalized cross correlation [41]. The accuracy of the estimates, in lateral and axial directions, was then evaluated for different frame rates and different velocities. In that study, in vitro experiments were carried out and the two methods were shown to be competitive in both image quality and motion estimation. DW imaging provided better image quality at limited depths, while MLT imaging performed better closer to the focal point. Similar STE axial errors were obtained for both methods, but DW provided better lateral estimates. However, as a phantom can hardly reproduce high intensity anatomical artifacts and clutter that comes from fat layers, ribs and lungs [42], which influence the STE accuracy, the aim of this study was to directly contrast both approaches in an in-vivo setting and to assess if the scan sequence may impact on the estimation of myocardial strain, i.e. the widely agreed final product of speckle tracking echocardiography, providing important clinical information on cardiac function.

In this paper, two scan sequences, one based on DWs and one on MLT, achieving the same maximum frame rate (833 Hz) were compared in HFR STE applications. First, images were recorded at baseline from healthy volunteers and patients. Next, additional acquisitions during stress echocardiography were performed on volunteers. Each scan was processed by a previously proposed 2D HFR STE [29] algorithm and strain curves and their end-systolic (ES) values were extracted for further comparison.

The paper is organized as follows: section II reports the in-vivo setup and presents the proposed framework and comparison process. Section III shows results obtained for both acquisition methods. Finally, further discussion together with final conclusions can be found in section IV.

## II. Methods

### A. Imaging setup

Images were acquired with the ULA-OP 256 scanner [43] connected to a phased array (model PA230, Esaote SpA, Florence, Italy), which has 128 elements (pitch = 170 μm), central frequency of 2MHz and −6 dB fractional-bandwidth of about 50%. 90°-wide, 144-line sector images with a depth range from 12 to 130 mm were obtained at a frame rate of 833 Hz by implementing two scan sequences based either on MLT or DW compounding. To achieve this, the ULA-OP 256 was set to consecutively acquire channel data - at a sampling rate of 19.5 MHz and a PRF of 5 kHz - for 2.48 s, i.e. 1.24 s for each scan sequence. Acquired data were then delay-and-sum beamformed in Matlab® (The MathWorks, Natick, MA).

MLT imaging was based on the transmission of 6 beams simultaneously focused along different directions at a focal distance of 70mm. A virtual source was placed behind the aperture centre at z=-5mm to maximize the transmitted energy along each direction, as well as to mitigate acoustic safety issues in the near field [44]. Moreover, to minimize motion artifacts between the 6 subsectors of the reconstructed image, the alternate ordering of transmission events proposed in [31] was applied. Finally, for each transmitted beam 4 lines were reconstructed in parallel.

On the other hand, DW imaging was based on the transmission of 6 DWs from 36-element wide sub-apertures apodized with a Tukey window. Each transmission had a virtual source placed behind the sub-aperture's centre at z=−2.42mm achieving an aperture angle of 90°. They were shifted on the x-direction in a triangular transmit sequence as suggested in [25]. Hence, the x-coordinates of the virtual sources were -7.82, -1.53, 4.76, 7.82, 1.53, -4.76mm, respectively. However, the images obtained from each diverging wave were coherently compounded without applying a motion correction technique as in [25], since the motion occurring during the transmission of 6 DWs at 5 kHz PRF (and thus the impact on the B-mode image quality) was considered negligible.

For a fair comparison and to avoid excessive probe surface heating, the acoustic output of both scan sequences was equalized as suggested in [38].

### B. In-vivo protocol

All cardiac images were acquired by an expert echocardiographer according to the protocol approved by the local ethics committee. Scans with the experimental scanner working in HFR imaging mode, as described in section IIA, were performed.

For the purpose of this study, apical 4-chamber views were recorded from 12 healthy volunteers and 5 patients, after signing informed consent. Volunteers were considered healthy when no cardiac pathology was reported in their medical history and the standard echocardiography and ECG did not highlight any pathology. Patients were recruited from the clinical patients treated at the cardiology department of UZ Leuven; among them, one was treated with chemotherapy, two had a myocardial inferior infarct, one was diagnosed with cardiac amyloidosis and the last one with arterial hypertension (left ventricle not hypertrophic). Each person, after resting a few minutes to stabilize the heart rate, laid on the left side and was scanned: first, with the MLT sequence; then, on the successive hearth beat, with the DW sequence. The acquisitions were repeated twice. The datasets acquired according to the above protocol will be referred to as the 'baseline' acquisitions.

A second dataset of acquisitions, referred to as 'stress test', was acquired on the volunteers by selecting 8 of them based on their image quality at rest. First, the day before the acquisition, the maximum workload was measured for each volunteer by an upright bicycle exercise test. Then, during the acquisition sessions, the volunteers were asked to cycle on the supine bicycle at three different workload levels: 25%, 50% and 66% of their maximum workload. The volunteer was cycling continuously, while the workload level was changed every 3 minutes: 2 minutes to stabilize the heart rate and 1 minute to acquire and download two datasets of HFR data.

### C. 2D motion estimator

For estimating the cardiac motion, our previously proposed 2D HFR STE algorithm was used [29]. Briefly, it is a 2-step estimator that computes axial and lateral displacement separately applying 1D cross-correlation on 2D kernels.

In the first step, the axial displacement is estimated. Two kernels (7°-wide and 4.5-mm high) of RF signals are extracted from the same position on consecutive frames and used as input for 1D cross-correlation. Then, with an axial overlap of 80% and a lateral shift of 1 line, the kernels are moved across the whole frame.

In the second step, the lateral displacement is calculated using 22°-wide and 7-mm high kernels of envelope data. Due to the lower lateral resolution and the fact that block matching better performs for displacements greater than one pixel, the kernels are not extracted from consecutive frames but between frames with a time lag of 30ms. To make sure that both kernels contain the same region of interest, the kernel on the search frame is shifted in the axial direction based on the estimation at the previous step.

For both steps, to achieve a subpixel precision, a 10:1 spline peak fitting is applied to the estimator.

### D. Strain estimation

#### 1) Contour tracking

Although the motion estimation was performed for the whole frame, only a subset of points, which were tracked throughout the cardiac cycle, was of interest for strain estimation. Hence, for each acquisition, an expert echocardiographer manually placed contour at myocardial mid-line on the frame at end-diastole. The starting contour (consisted of ~108 points) was set either on the MLT or DW image, randomly chosen, and applied to both images to avoid final estimates to be contour dependent. Moreover, to improve the tracking-robustness 8 other contours were automatically selected by expanding and contracting the manually selected one on a band of 4 mm for all 17 subjects (Fig. 1), i.e. each contour was offset by 0.5 mm from the previous one. All 9 contours were tracked separately between all frames and the motion of the main contour was defined as an average position of the region of interest (ROI).

As those points were tracked independently, considering both axial and lateral displacement, an unnatural motion of the contour could occur. Therefore, the positions of the tracked points were connected by a spline, which was smoothed by a Savitzky-Golay filter [45] in order to minimize the least-squares error in fitting a polynomial to windows of noisy data. For the purpose of this work a 2nd order polynomial and a 11-point wide window was used. The filter was empirically set to avoid unnatural motion of the contour [29].

#### 2) Segmental Longitudinal Strain

The myocardial tracking contour was divided into six segments according to the recommended guidelines of the European Association of Cardiovascular Imaging (EACVI) / American Society of Echocardiography (ASE) [46]. For each segment, the strain was calculated as a simple percent length change of the contour [47] as follows:

$$S(t) = \frac{L(t) - L_0}{L_0} \quad (1)$$

where $L(t)$ is the length of the contour of the specific segment at time instance $t$ and $L_0$ is its initial length, i.e. at end-diastole.

For further statistical analysis, end-systolic (ES) strain values were extracted, where the ES time was defined as the first zero-

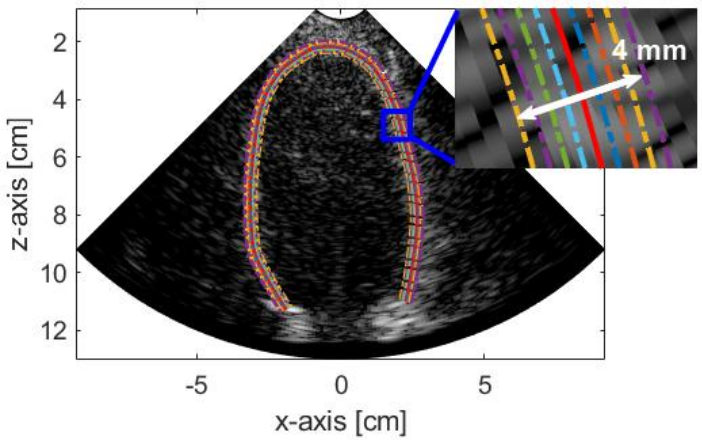


Fig. 1 Main contour (solid red line) with 8 additional contours to improve the robustness of the algorithm. The distance between two contours was set to 0.5 mm. The contour is split in 6 segments: BS – basal septum, MS – mid septum, AS – apical septum, ALW – apical lateral wall, MLW – mid lateral wall, BLW – basal lateral wall.

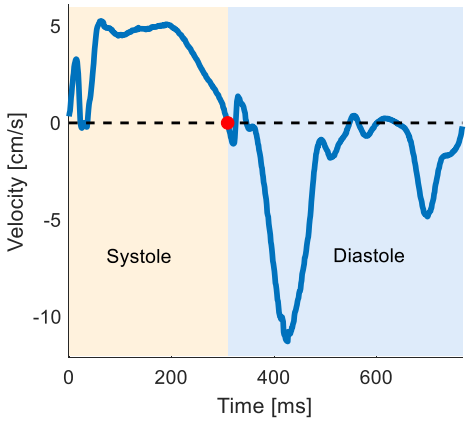


Fig. 2 Example of velocity curve estimated on the mid septum and end-systolic time (red dot).

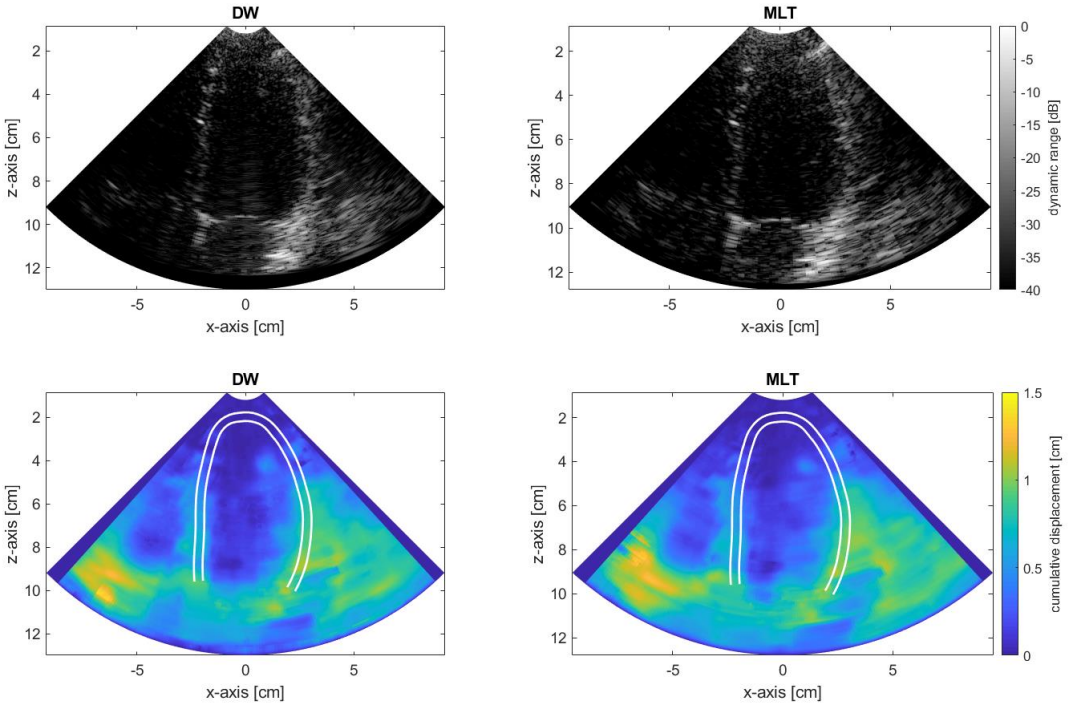


Fig. 3 B-mode images (top) and magnitude of the cumulative displacement (bottom) at ES time obtained by DW (left) and MLT (right) scan sequences. White lines on the displacement fields mark the contour which was placed on the left ventricle.

crossing time of the velocity curve, estimated on the mid septum, happening after the systolic peak (Fig. 2). Specifically, the ES time was, first, semi-automatically and separately extracted on both DW and MLT scans; then, the two estimated values were averaged to improve robustness and to avoid that differences in strain ES values could have been biased by slightly different ES times. Since, potentially, two consecutive heartbeats could be slightly different, the correctness of the estimated ES time was visually checked for each scan and if necessary adjusted.

### *E. Statistical analysis*

After processing all the scans, the videos with tracked ROI were saved for feasibility assessment performed by the expert echocardiographer. Specifically, the same scan using both HFR scan sequences was shown to the echocardiographer and segments were labeled as ‘tracked’ or ‘non-tracked’ based on her expertise and the visual readings.

To contrast the results obtained with both sequences, a two-way analysis of variance (ANOVA) with a repeated measures design and Bonferroni post-hoc analysis was performed on the ES values. A p-value $<0.05$ was considered statistically significant. For each set of acquisitions, i.e. baseline and stress test, ANOVA was performed twice:

1) for all the data regardless of the tracking performance
2) only for the segments labeled as ‘tracked’.

The baseline set was used to analyze the influence of the scan sequence and position of the segment within the image (i.e. apical, mid, and basal). Moreover, the stress test set was used to assess the impact of overall image quality (which decreases during stress) on both scan sequences.

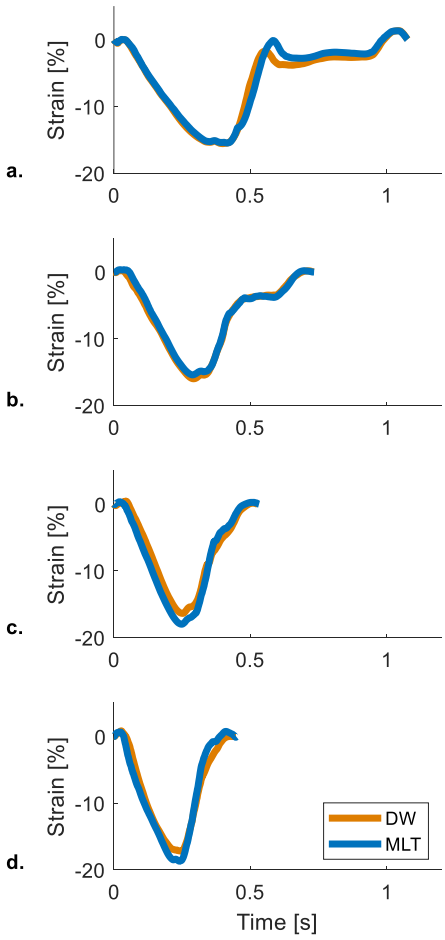


Fig. 4 Example of global strain obtained at (a) baseline, (b) 25%, (c) 50% and (d) 66% of max workload.

TABLE I FEASIBILITY OF THE TWO SCAN MODES AT BASELINE FOR ALL SUBJECTS.

| | | *DW* | *MLT* | Agreement |
|---|---|---|---|---|
| **Segments** | Apical | 19% | 18% | 99% |
| | Mid | 72% | 65% | 91% |
| | Basal | 71% | 69% | 90% |
| **Walls** | Septum | 69% | 65% | 97% |
| | Lateral Wall | 39% | 36% | 90% |
| | **Average** | **54%** | **51%** | **93%** |

## III. RESULTS

### A. *Qualitative comparison*

Fig. 3 shows an example of B-mode images and cumulative displacement at ES time obtained by MLT and DW scan sequences. Qualitatively, B-mode images were very similar, as also shown in the supplementary accompanying video clip . In both cases the septum was usually well visible, while the lateral wall had lower visibility, except for the basal segment which was very bright. Moreover, both scan sequences presented similar image quality; the same type of artifacts were observed, e.g. the apical region was heavily influenced by near field clutter. However, due to the parallel beamforming of 4 lines per beam in the MLT approach, 4-line pattern discontinuity was visible on the B-mode images. It is worth highlighting that these images are raw MLA images. Nevertheless, with a slightly higher computational load, the so-called synthetic transmit beam could be implemented, which was shown effective to remove such an artifacts [38]. On the other hand, in DW images, some noisy lines were present (see the line in Fig. 3 passing through (0, 12) cm), which were due to switching noise that interferes constructively in this specific configuration of the system. Furthermore, the cumulative displacement fields obtained at the ES time (Fig. 3 bottom) were very similar, especially along the myocardium (white lines). Visually, there were some small differences in the images, which could be due to different artifacts patterns and to a slightly different myocardial motion on consecutive heartbeats.

The estimated global strain curves showed a physiological pattern for both imaging methods (Fig. 4). During stress test, as expected, higher heart rates corresponded to shorter total time of deformation and slightly higher strain values. In addition, the diastolic part of the curve (diastasis), consistently shortening with increasing heart rate, changed its shape between stages. Nevertheless, no obvious differences could be seen between the patterns obtained with both methods.

### B. *Baseline*

Table I shows the tracking feasibility for both scan sequences and highlights the feasibility dependency with respect to different depths (apical, mid, basal) and position on the image (lateral wall/septum). It could be observed that the percentage of segments that are labeled as 'tracked' was slightly higher for DW (54% vs 51% in average). The same trend was shown for both septum and lateral walls. On the segmental level, the biggest difference was present in the mid segments, where 72% of the segments were correctly tracked on DW scans and 65% on MLT scans. A smaller difference could be seen in the basal segments (71% for DW and 69% for MLT). Finally, the feasibility of the apical segments was very similar (19% for DW and 18% for MLT). However, the latter was the lowest among the segments likely due to strong near field artifacts that were present in both approaches. Moreover, Table I shows that the tracking agreement between DW and MLT, i.e. the percentage of segments having the same label for both scan sequences, was ranging from 90% to 99%. The smallest agreement was present in the lateral wall and basal segments (90%), while apical segments were equally labeled in 99% of the cases, most likely because a lot of them were labeled as 'non-tracked'.

The ANOVA analysis showed that the comparison between ES values from all segments obtained with both scan sequences (Fig. 5) showed a clear difference from base to apex ($p<0.03$), but did not reveal differences between acquisition modes ($p>0.96$) nor interactions between segments and acquisition

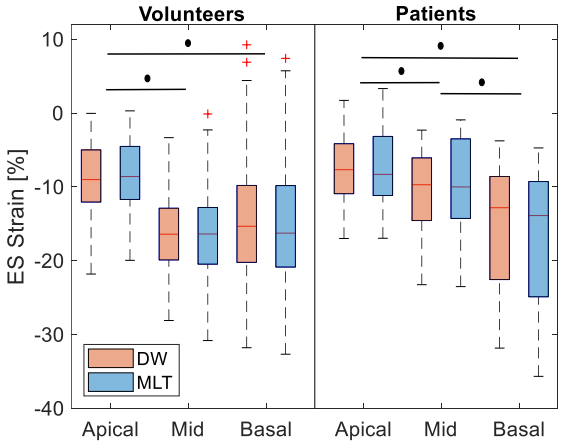


Fig. 5 Comparison between ES values from all segments obtained with both scan sequences at baseline. * p< 0.03

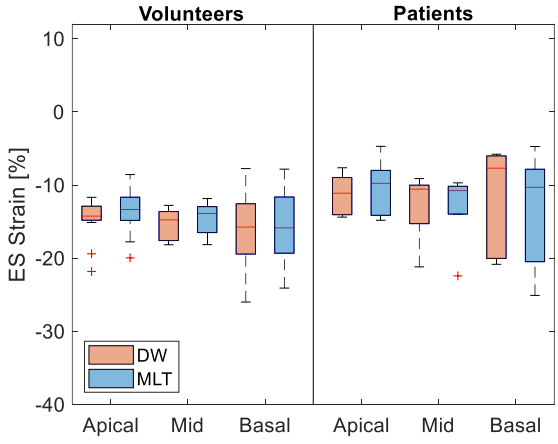


Fig. 6 Comparison between ES values from tracked segments obtained with both scan sequences at baseline.

TABLE II FEASIBILITY OF THE TWO SCAN MODES UNDER DIFFERENT STRESS LEVELS.

| | | 25% of max workload | | | 50% of max workload | | | 66% of max workload | | |
|---|---|---|---|---|---|---|---|---|---|---|
| | | *DW* | *MLT* | Agreement | *DW* | *MLT* | Agreement | *DW* | *MLT* | Agreement |
| **Segments** | Apical | 22% | 13% | 91% | 13% | 9% | 97% | 9% | 13% | 97% |
| | Mid | 78% | 69% | 91% | 66% | 53% | 88% | 28% | 31% | 97% |
| | Basal | 84% | 75% | 91% | 59% | 59% | 81% | 25% | 34% | 91% |
| **Walls** | Septum | 69% | 63% | 94% | 63% | 56% | 85% | 35% | 38% | 98% |
| | Lateral Wall | 54% | 42% | 88% | 29% | 25% | 92% | 6% | 15% | 92% |
| | **Average** | **61%** | **52%** | **91%** | **46%** | **41%** | **89%** | **21%** | **26%** | **95%** |

mode (p>0.57). Limiting the analysis to the 'tracked' segments only (Fig. 6) made the difference between segments no longer significant (p>0.3), but did not change the result between scan sequences (p>0.35) nor the interaction between segments and acquisition mode (p>0.87). Finally, the mean ES values were similar among the segments with a slightly higher variance for basal segments. Specifically, the apical ES value obtained for volunteers was -14.7±2.8% for DW and -13.4±3.1% for MLT while, for patients, it was -11.3±2.6% for DW and -10.5±3.6% for MLT. For the mid segments, values were slightly lower -15.4±2% vs. -14.6±2.1% for DW and MLT, respectively, for volunteers and -12.9±4.4% vs. -12.9±4.8% for patients. Finally, as mentioned before, the basal segments were characterized by bigger variances ±5 % for DW and ±4.7% for MLT for volunteers and ±6.8% for DW and ±7.4% for MLT for patients.

### C. *Bicycle*

Feasibility of the two scan modes across different stress levels are reported in Table II. The agreement presented high values (>80%) at all stress levels. On the other hand, the feasibility was decreasing with the increasing stress level. Moreover, at each stage the feasibility was higher in the septum than in the lateral wall (e.g. 69% vs 54% for first stage). Finally, a slightly better performance was seen for the DW sequence in the two first stages, while the relation was inverted for the last stress level and MLT obtained slightly higher feasibility. A similar trend was present among all segments.

ANOVA was performed on ES values from all segments ('tracked' as well as 'non-tracked') during stress testing (Fig. 7) and showed similar results to the one obtained with baseline images: a significant difference between segments (p<0.0001) and no significance between scan sequences (p>0.44) nor interactions between these two factors (p>0.22). Next, the ES values from correctly tracked segments were extracted. Unfortunately, due to low feasibility, especially in the apical region, it was not possible to run a statistical analysis separately for each stage. Hence, all the values were put together before performing the ANOVA test (Fig. 8). Again, no significance between segments (p=0.08), modes (p=0.83) or in the interaction (p=0.45) were found. Finally, the mean ES values during stress testing obtained from DW images were -18.9±4.3% for apical segments, -19.8±3% for mid segments and -18.2±6.1% for basal. Similarly, for MLT scans the mean ES values were -17.9±3.6%, -22.2±4.2% and -17.6±4.3% for apical, mid, and basal segments, respectively.

## IV. DISCUSSION AND CONCLUSION

In this paper, MLT and DW scan sequences, i.e. the most widely used sequences for HFR echocardiography, were compared in an in-vivo setting for HFR STE applications. First, the two scan sequences were compared at resting condition (called baseline), for which the heart rate and the position of the

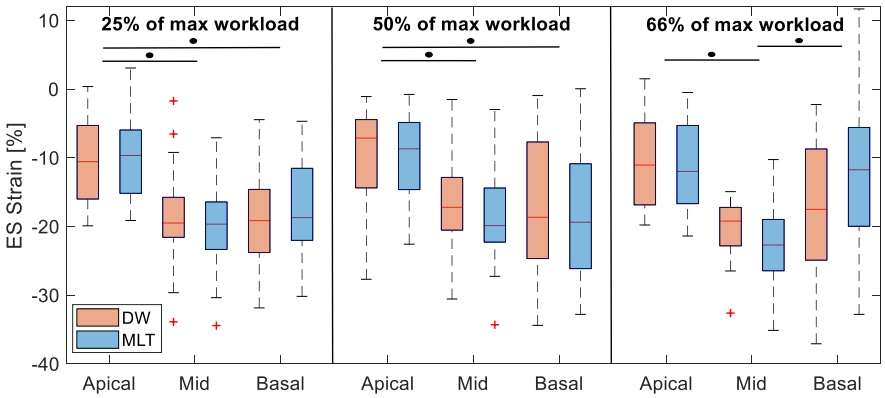


Fig. 7 Comparison between ES values from all segments obtained with both scan sequences during stress testing. * p<0.0001

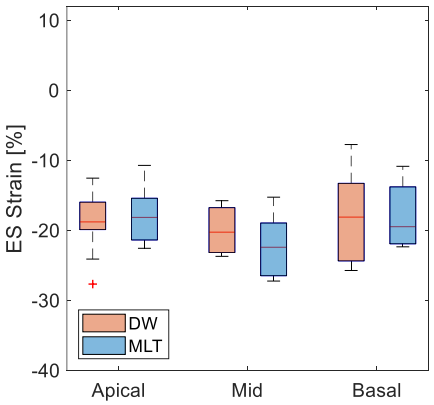


Fig. 8 Comparison between ES values from tracked segments obtained with both scan sequence for all stress levels.

volunteer were optimal to obtain the best possible image quality. Then, an additional set of images (called stress test) was taken, on a subgroup of volunteers, under challenging scanning conditions. Specifically, the volunteers were cycling, eventually panting, on the supine bicycle during acquisition, thus making it difficult to find a good and stable imaging window. Moreover, increased heart rate and breathing introduced faster movements and more artifacts on the images. MLT and DW scan sequences were quantitatively compared in terms of STE feasibility and estimated ES strain values. A statistical analysis was finally conducted to examine the influence of the scan sequence and the position of the segment within the image.

The strain curves obtained from tracking motion on images from both acquisition methods were similar and had a physiological pattern (Fig. 4). Visually, the scans had equally good image quality, wall visibility and similar type of artifacts. However, a small discontinuity due to parallel beamforming was noticeable for MLT. Even if this discontinuity could have been alleviated by implementing the so-called synthetic transmit beams (STB, [48]), it would have doubled the computational burden of beamforming and, hence, it was not considered in this study. The better uniformity of DW images might have had an impact on STE feasibility, which was slightly higher than for MLT (54% vs 51%, respectively) although this difference is marginal particularly in the light of a single observer rating the tracking quality. In any case, even if different scan sequences might have an impact on displacement estimates, they did not condition the clinically relevant strain parameters. Indeed, ES values were not significantly different between the sequences, as shown in Fig. 5 and Fig. 6.

The feasibility in the stress test set varied a little bit more (see Table II). This happened mostly due to quick changes of image scenery. While cycling, the body was moving slightly, the heart rate was increasing and the volunteer was breathing faster and heavier. Especially in the last stages (50% and 66% of the maximum workload), even if the volunteers were asked to hold their breath during the acquisition time, heavy breathing could have caused differences in image quality. Moreover, breathing and the sweat on the volunteer's skin could impair the stability of the probe position, which could slightly change during the acquisition (particularly true for the DW scan sequence, which was always acquired after MLT). The above reasons could partially explain why there is an inverted trend between DW and MLT observed at 66% of maximum workload (21% vs 26% respectively). Nevertheless, due to the low feasibility at these workload levels, we cannot give a definitive explanation. Due to all the challenges mentioned above, the feasibility dropped from 61% and 52% (at 25% of max workload) to 21% and 26% (at the last stage) for DW and MLT approaches, respectively. This trend was expected, since the decrease of feasibility was already reported in the literature, even for high-end clinical scanners running conventional (i.e. high SNR) image sequences [49]. On the other hand, it is worth mentioning that the feasibility of the baseline dataset was lower than the one obtained with the stress test dataset at 25% of max workload (54% and 51% vs 61% and 52% for DW and MLT respectively). This can be explained by two factors. First, as it was mentioned above, the volunteers were selected based on image quality and only 8 volunteers with good image quality were recruited for additional scans. Secondly, light exercising at the beginning of the stress test caused only a slight increase of the heart rate without compromising the image quality with breathing artifacts.

In addition to feasibility, the agreement, i.e. the percentage of segments labeled the same for both approaches, was calculated. The results showed that the value was always higher than 89% on average, ranging for segments from 81% to 99%. Furthermore, taking into account scans from both sets, the agreement between MLT and DW was 92%. This suggests that, most likely, the feasibility was not impacted by the used approach (MLT or DW), but mainly by the small differences in the view, position, artifacts, and clutter.

In both sets the statistical analysis showed statistically significant difference between segments (from base to apex) when all the ES values were used despite of the tracking performance (see Fig. 5 and Fig. 7). This was caused by the influence of the non-tracked segments. Indeed, for 'non-tracked' segments, STE detected a reduced motion compared to what could be qualitatively seen on the image, thus giving lower ES values than expected. Hence, the limited STE feasibility on apical segments (~19%, for the baseline dataset) biased ES values to lower values. Such a big difference in the feasibility across the segments was caused by the clutter and artifacts present at different depths. Especially, the first 3 cm of the images were mostly affected by strong near field clutter.

One of the limitations of this study is the number of tested cases. Although the initial number is quite high, i.e.100 values per segment at baseline ((17 subjects + 8 volunteer scanned at rest on the bicycle)×2 acquisitions × 2 walls) and 96 for stress test, i.e. 32 per stage, the feasibility of apical segments was low (ranging from 22% to 9%). Hence, when only the tracked segments are considered in the ANOVA test, since it requires the same amount of data per group, only 18 values per segment could be used for baseline and only 3 for each stage in stress test. That is why in stress test set, the comparison between ES values from tracked segments, the stages were combined to be able to perform statistical testing. The issue could be solved by recruiting more volunteers/patients or by increasing the feasibility. The latter could be done either by improving the speckle tracking algorithm or by enhancing the image quality, e.g. by applying advanced clutter filtering techniques.

Moreover, the mean ES values from the tracked segments, estimated with our method, are slightly lower in magnitude (see Fig. 6) than those described in the literature [50]. Indeed, since the quality of HFR images is low (see Fig. 3), our ES values are affected by the limited visibility of the myocardium, especially along the lateral wall where we mainly estimate the epicardial strain, which is known to be smaller [51].

Overall, our findings show that MLT and DW compounding give comparable HFR STE strain values and that the choice for using one method or the other may be rather based on other factors such as: system requirements, computational load, energy transfer to the body, achievable frame rate, motion artifacts and image quality. Specifically, the implementation of MLT sequences requires, in transmission, arbitrary waveform generators and a different signal for each active element, which could increase the complexity of the electronic circuitry and the amount of control logic for the management of the transmitter. On the other hand, MLT needs a less performing beamformer

than DW. Indeed, in our case, for each transmission event 16 lines were reconstructed in parallel for MLT and 144 lines for DW, i.e. the whole image. At the same time, however, the DW approach allows higher frame rate, which, in principle, could be limited only by the PRF, when no compounding is implemented but – obviously – at the cost of spatial resolution and contrast-to-noise ratio.

In addition, motion artifacts can impact STE as they appear due to the time needed to reconstruct a whole frame. In DW imaging, the intensity of quickly moving anatomical structures could be reduced by the inherent low-pass effect of compounding; in MLT imaging, motion could produce speckle discontinuities at the borders of the subsectors in which the image is split.

Furthermore, it is also worth mentioning that the main issue for patient safety in HFR imaging is heating of the probe surface [38] and MLT and DW produce different mechanical/thermal indexes and attenuated spatial-peak temporal-average intensity. In general, for the same probe temperature, wide DWs have lower values of patient safety indexes, but it could be worse in harmonic imaging where a higher mechanical index is required. Finally, even if we showed that the image quality is comparable, at least qualitatively, there could be artifacts reduction techniques that may improve the image quality in a different way for the two scan sequences. For example, SVD filters may be implemented for DW before compounding (while this cannot be done for MLT) or as it was already mentioned STB could be implemented to improve MLT image appearance.

Future studies will focus on short-lived events of interest which could be of relevance to study mechanical activation wavefronts, systolic and/or diastolic function.

## V. References

[1] K. Kalam, P. Otahal, and T. H. Marwick, "Prognostic implications of global LV dysfunction: a systematic review and meta-analysis of global longitudinal strain and ejection fraction," *Heart Br. Card. Soc.*, vol. 100, no. 21, pp. 1673–1680, Nov. 2014, doi: 10.1136/heartjnl-2014-305538.

[2] J. Gorcsan and H. Tanaka, "Echocardiographic Assessment of Myocardial Strain," *J. Am. Coll. Cardiol.*, vol. 58, no. 14, pp. 1401–1413, Sep. 2011, doi: 10.1016/j.jacc.2011.06.038.

[3] M. Dandel, H. Lehmkuhl, C. Knosalla, N. Suramelashvili, and R. Hetzer, "Strain and Strain Rate Imaging by Echocardiography – Basic Concepts and Clinical Applicability," *Curr. Cardiol. Rev.*, vol. 5, no. 2, pp. 133–148, May 2009, doi: 10.2174/157340309788166642.

[4] W. N. McDicken, G. R. Sutherland, C. M. Moran, and L. N. Gordon, "Colour Doppler velocity imaging of the myocardium," *Ultrasound Med. Biol.*, vol. 18, no. 6–7, pp. 651–654, 1992.

[5] E. D. Angelini and O. Gerard, "Review of Myocardial Motion Estimation Methods from Optical Flow Tracking on Ultrasound Data," in *2006 International Conference of the IEEE Engineering in Medicine and Biology Society*, Aug. 2006, pp. 1537–1540, doi: 10.1109/IEMBS.2006.259640.

[6] N. L. Greenberg *et al.*, "Doppler-derived myocardial systolic strain rate is a strong index of left ventricular contractility," *Circulation*, vol. 105, no. 1, pp. 99–105, Jan. 2002.

[7] B. Chakraborty, Z. Liu, B. Heyde, J. Luo, and J. D'hooge, "2-D Myocardial Deformation Imaging Based on RF-Based Nonrigid Image Registration," *IEEE Trans. Ultrason. Ferroelectr. Freq. Control*, vol. 65, no. 6, pp. 1037–1047, 2018, doi: 10.1109/TUFFC.2018.2821902.

[8] P. Lancellotti *et al.*, "Importance of left ventricular longitudinal function and functional reserve in patients with degenerative mitral regurgitation: assessment by two-dimensional speckle tracking," *J. Am. Soc. Echocardiogr. Off. Publ. Am. Soc. Echocardiogr.*, vol. 21, no. 12, pp. 1331–1336, Dec. 2008, doi: 10.1016/j.echo.2008.09.023.

[9] A. B. Nielsen *et al.*, "Usefulness of left atrial speckle tracking echocardiography in predicting recurrence of atrial fibrillation after radiofrequency ablation: a systematic review and meta-analysis," *Int. J. Cardiovasc. Imaging*, Apr. 2020, doi: 10.1007/s10554-020-01828-2.

[10] H.-Y. Liang *et al.*, "Usefulness of two-dimensional speckle strain for evaluation of left ventricular diastolic deformation in patients with coronary artery disease," *Am. J. Cardiol.*, vol. 98, no. 12, pp. 1581–1586, Dec. 2006, doi: 10.1016/j.amjcard.2006.07.038.

[11] H. Shi *et al.*, "Longitudinal two-dimensional strain rate imaging: a potential approach to predict the response to cardiac resynchronization therapy," *Int. J. Cardiovasc. Imaging*, vol. 25, no. 7, pp. 677–687, Oct. 2009, doi: 10.1007/s10554-009-9480-z.

[12] J. Gorcsan *et al.*, "Echocardiography for Cardiac Resynchronization Therapy: Recommendations for Performance and Reporting–A Report from the American Society of Echocardiography Dyssynchrony Writing Group Endorsed by the Heart Rhythm Society," *J. Am. Soc. Echocardiogr.*, vol. 21, no. 3, pp. 191–213, Mar. 2008, doi: 10.1016/j.echo.2008.01.003.

[13] G. Ansalone, P. Giannantoni, R. Ricci, P. Trambaiolo, F. Fedele, and M. Santini, "Doppler myocardial imaging to evaluate the effectiveness of pacing sites in patients receiving biventricular pacing," *J. Am. Coll. Cardiol.*, vol. 39, no. 3, pp. 489–499, Feb. 2002, doi: 10.1016/S0735-1097(01)01772-7.

[14] Penicka Martin *et al.*, "Improvement of Left Ventricular Function After Cardiac Resynchronization Therapy Is Predicted by Tissue Doppler Imaging Echocardiography," *Circulation*, vol. 109, no. 8, pp. 978–983, Mar. 2004, doi: 10.1161/01.CIR.0000116765.43251.D7.

[15] M. Cikes, L. Tong, G. R. Sutherland, and J. D'hooge, "Ultrafast Cardiac Ultrasound Imaging: Technical Principles, Applications, and Clinical Benefits," *JACC Cardiovasc. Imaging*, vol. 7, no. 8, pp. 812–823, Aug. 2014, doi: 10.1016/j.jcmg.2014.06.004.

[16] H. Kanai, "Propagation of spontaneously actuated pulsive vibration in human heart wall and in vivo viscoelasticity estimation," *IEEE Trans. Ultrason. Ferroelectr. Freq. Control*, vol. 52, no. 11, pp. 1931–1942, Nov. 2005, doi: 10.1109/TUFFC.2005.1561662.

[17] D. P. Shattuck, M. D. Weinshenker, S. W. Smith, and O. T. von Ramm, "Explososcan: A parallel processing technique for high speed ultrasound imaging with linear phased arrays," *J. Acoust. Soc. Am.*, vol. 75, no. 4, pp. 1273–1282, Apr. 1984, doi: 10.1121/1.390734.

[18] L. Demi, "Practical Guide to Ultrasound Beam Forming: Beam Pattern and Image Reconstruction Analysis," *Appl. Sci.*, vol. 8, no. 9, Art. no. 9, Sep. 2018, doi: 10.3390/app8091544.

[19] I. K. Ekroll, A. Swillens, P. Segers, T. Dahl, H. Torp, and L. Lovstakken, "Simultaneous quantification of flow and tissue velocities based on multi-angle plane wave imaging," *IEEE Trans. Ultrason. Ferroelectr. Freq. Control*, vol. 60, no. 4, pp. 727–738, Apr. 2013, doi: 10.1109/TUFFC.2013.2621.

[20] B. Denarie *et al.*, "Coherent Plane Wave Compounding for Very High Frame Rate Ultrasonography of Rapidly Moving Targets," *IEEE Trans. Med. Imaging*, vol. 32, no. 7, pp. 1265–1276, Jul. 2013, doi: 10.1109/TMI.2013.2255310.

[21] J. Jensen, M. B. Stuart, and J. A. Jensen, "Optimized Plane Wave Imaging for Fast and High-Quality Ultrasound Imaging," *IEEE Trans. Ultrason. Ferroelectr. Freq. Control*, vol. 63, no. 11, pp. 1922–1934, Nov. 2016, doi: 10.1109/TUFFC.2016.2591980.

[22] C. Papadacci, M. Pernot, M. Couade, M. Fink, and M. Tanter, "High-contrast ultrafast imaging of the heart," *IEEE Trans. Ultrason. Ferroelectr. Freq. Control*, vol. 61, no. 2, pp. 288–301, Feb. 2014, doi: 10.1109/TUFFC.2014.6722614.

[23] P. Joos *et al.*, "High-Frame-Rate Speckle-Tracking Echocardiography," *IEEE Trans. Ultrason. Ferroelectr. Freq. Control*, vol. 65, no. 5, pp. 720–728, 2018, doi: 10.1109/TUFFC.2018.2809553.

[24] H. Hasegawa and H. Kanai, "High-frame-rate echocardiography using diverging transmit beams and parallel receive beamforming," *J. Med. Ultrason. 2001*, vol. 38, no. 3, pp. 129–140, Jul. 2011, doi: 10.1007/s10396-011-0304-0.

[25] J. Poree, D. Posada, A. Hodzic, F. Tournoux, G. Cloutier, and D. Garcia, "High-Frame-Rate Echocardiography Using Coherent Compounding With Doppler-Based Motion-Compensation," *IEEE Trans. Med. Imaging*, vol. 35, no. 7, pp. 1647–1657, Jul. 2016, doi: 10.1109/TMI.2016.2523346.

[26] M. Toulemonde *et al.*, "High-Frame-Rate Contrast Echocardiography Using Diverging Waves: Initial In Vitro and In Vivo Evaluation," *IEEE Trans. Ultrason. Ferroelectr. Freq. Control*, vol. 65, no. 12, pp. 2212–2221, Dec. 2018, doi: 10.1109/TUFFC.2018.2856756.

[27] J. Grondin, V. Sayseng, and E. E. Konofagou, "Cardiac Strain Imaging With Coherent Compounding of Diverging Waves," *IEEE Trans. Ultrason. Ferroelectr. Freq. Control*, vol. 64, no. 8, pp. 1212–1222, Aug. 2017, doi: 10.1109/TUFFC.2017.2717792.

[28] J. Porée, M. Baudet, F. Tournoux, G. Cloutier, and D. Garcia, "A Dual Tissue-Doppler Optical-Flow Method for Speckle Tracking Echocardiography

at High Frame Rate," *IEEE Trans. Med. Imaging*, vol. 37, no. 9, pp. 2022–2032, Sep. 2018, doi: 10.1109/TMI.2018.2811483.
[29] M. Orlowska *et al.*, "A novel 2D speckle tracking method for high frame rate echocardiography," *IEEE Trans. Ultrason. Ferroelectr. Freq. Control*, pp. 1–1, 2020, doi: 10.1109/TUFFC.2020.2985451.
[30] L. Tong, H. Gao, and J. D'hooge, "Multi-transmit beam forming for fast cardiac imaging--a simulation study," *IEEE Trans. Ultrason. Ferroelectr. Freq. Control*, vol. 60, no. 8, pp. 1719–1731, Aug. 2013, doi: 10.1109/TUFFC.2013.2753.
[31] A. Ramalli *et al.*, "Real-Time High-Frame-Rate Cardiac B-Mode and Tissue Doppler Imaging Based on Multiline Transmission and Multiline Acquisition," *IEEE Trans. Ultrason. Ferroelectr. Freq. Control*, vol. 65, no. 11, pp. 2030–2041, Nov. 2018, doi: 10.1109/TUFFC.2018.2869473.
[32] A. Rabinovich, A. Feuer, and Z. Friedman, "Multi-line transmission combined with minimum variance beamforming in medical ultrasound imaging," *IEEE Trans. Ultrason. Ferroelectr. Freq. Control*, vol. 62, no. 5, pp. 814–827, May 2015, doi: 10.1109/TUFFC.2014.006754.
[33] G. Zurakhov, Z. Friedman, D. S. Blondheim, and D. Adam, "High-Resolution Fast Ultrasound Imaging With Adaptive-Lag Filtered Delay-Multiply-and-Sum Beamforming and Multiline Acquisition," *IEEE Trans. Ultrason. Ferroelectr. Freq. Control*, vol. 66, no. 2, pp. 348–358, Feb. 2019, doi: 10.1109/TUFFC.2018.2886182.
[34] F. Prieur, B. Dénarié, A. Austeng, and H. Torp, "Correspondence - Multi-line transmission in medical imaging using the second-harmonic signal," *IEEE Trans. Ultrason. Ferroelectr. Freq. Control*, vol. 60, no. 12, pp. 2682–2692, Dec. 2013, doi: 10.1109/TUFFC.2013.2868.
[35] G. Matrone, A. Ramalli, J. D'hooge, P. Tortoli, and G. Magenes, "A Comparison of Coherence-Based Beamforming Techniques in High-Frame-Rate Ultrasound Imaging With Multi-Line Transmission," *IEEE Trans. Ultrason. Ferroelectr. Freq. Control*, vol. 67, no. 2, pp. 329–340, 2020, doi: 10.1109/TUFFC.2019.2945365.
[36] L. Tong *et al.*, "Coded Excitation for Crosstalk Suppression in Multi-line Transmit Beamforming: Simulation Study and Experimental Validation," *Appl. Sci.*, vol. 9, no. 3, Art. no. 3, Jan. 2019, doi: 10.3390/app9030486.
[37] S. Vedula *et al.*, "High quality ultrasonic multi-line transmission through deep learning," *MLMIR@MICCAI*, 2018, doi: 10.1007/978-3-030-00129-2_17.
[38] A. Ramalli, A. Rodriguez-Molares, J. Avdal, J. D'hooge, and L. Løvstakken, "High-Frame-Rate Color Doppler Echocardiography: A Quantitative Comparison of Different Approaches," *IEEE Trans. Ultrason. Ferroelectr. Freq. Control*, vol. 67, no. 5, pp. 923–933, May 2020, doi: 10.1109/TUFFC.2019.2958031.
[39] A. Ramalli *et al.*, "High-Frame-Rate Tri-Plane Echocardiography With Spiral Arrays: From Simulation to Real-Time Implementation," *IEEE Trans. Ultrason. Ferroelectr. Freq. Control*, vol. 67, no. 1, pp. 57–69, Jan. 2020, doi: 10.1109/TUFFC.2019.2940289.
[40] E. Badescu *et al.*, "Comparison Between Multiline Transmission and Diverging Wave Imaging: Assessment of Image Quality and Motion Estimation Accuracy," *IEEE Trans. Ultrason. Ferroelectr. Freq. Control*, vol. 66, no. 10, pp. 1560–1572, Oct. 2019, doi: 10.1109/TUFFC.2019.2925581.
[41] I. A. Hein and W. D. O'Brien, "Current time-domain methods for assessing tissue motion by analysis from reflected ultrasound echoes-a review," *IEEE Trans. Ultrason. Ferroelectr. Freq. Control*, vol. 40, no. 2, pp. 84–102, Mar. 1993, doi: 10.1109/58.212556.
[42] A. Fatemi, E. A. R. Berg, and A. Rodriguez-Molares, "Studying the Origin of Reverberation Clutter in Echocardiography: In Vitro Experiments and In Vivo Demonstrations," *Ultrasound Med. Biol.*, vol. 45, no. 7, pp. 1799–1813, Jul. 2019, doi: 10.1016/j.ultrasmedbio.2019.01.010.
[43] E. Boni *et al.*, "Architecture of an Ultrasound System for Continuous Real-Time High Frame Rate Imaging," *IEEE Trans. Ultrason. Ferroelectr. Freq. Control*, vol. 64, no. 9, pp. 1276–1284, Sep. 2017, doi: 10.1109/TUFFC.2017.2727980.
[44] P. Santos, L. Tong, A. Ortega, L. Løvstakken, E. Samset, and J. D'hooge, "Acoustic output of multi-line transmit beamforming for fast cardiac imaging: a simulation study," *IEEE Trans. Ultrason. Ferroelectr. Freq. Control*, vol. 62, no. 7, pp. 1320–1330, Jul. 2015, doi: 10.1109/TUFFC.2015.006996.
[45] A. Savitzky and M. Golay, "Smoothing and Differentiation of Data by Simplified Least Squares Procedures," *Anal. Chem.*, vol. 36, pp. 1627–1639, Jul. 1964, doi: 10.1021/ac60214a047.
[46] J.-U. Voigt *et al.*, "Definitions for a common standard for 2D speckle tracking echocardiography: consensus document of the EACVI/ASE/Industry Task Force to standardize deformation imaging," *Eur. Heart J. Cardiovasc. Imaging*, vol. 16, no. 1, pp. 1–11, Jan. 2015, doi: 10.1093/ehjci/jeu184.
[47] J. D'hooge *et al.*, "Regional strain and strain rate measurements by cardiac ultrasound: principles, implementation and limitations," *Eur. J. Echocardiogr. J. Work. Group Echocardiogr. Eur. Soc. Cardiol.*, vol. 1, no. 3, pp. 154–170, Sep. 2000, doi: 10.1053/euje.2000.0031.
[48] T. Hergum, T. Bjastad, K. Kristoffersen, and H. Torp, "Parallel beamforming using synthetic transmit beams," *IEEE Trans. Ultrason. Ferroelectr. Freq. Control*, vol. 54, no. 2, pp. 271–280, Feb. 2007, doi: 10.1109/TUFFC.2007.241.
[49] C. C. Caniggia *et al.*, "Feasibility and Contribution of Global and Regional 2D Strain during Exercise Stress Echocardiography," *Argent. J. Cardiol.*, vol. 82, no. 2, Art. no. 2, Feb. 2014, doi: 10.7775/ajc.82.2.2701.
[50] H. Dalen *et al.*, "Segmental and global longitudinal strain and strain rate based on echocardiography of 1266 healthy individuals: the HUNT study in Norway," *Eur. J. Echocardiogr.*, vol. 11, no. 2, pp. 176–183, Mar. 2010, doi: 10.1093/ejechocard/jep194.
[51] Y. Nagata, V. C.-C. Wu, Y. Otsuji, and M. Takeuchi, "Normal range of myocardial layer-specific strain using two-dimensional speckle tracking echocardiography," *PloS One*, vol. 12, no. 6, p. e0180584, 2017, doi: 10.1371/journal.pone.0180584.